Computational and Mathematical Methods in Medicine
Vol. 10, No. 4, December 2009, 241–252

Taylor & Francis
Taylor & Francis Group

Correlation between animal and mathematical models for prostate cancer progression

Z. Jackiewicz[a1], C.L. Jorcyk[b2], M. Kolev[c3] and B. Zubik-Kowal[d4]*

[a]*Department of Mathematics and Statistics, Arizona State University, Tempe, AZ, USA;* [b]*Department of Biology, Boise State University, Boise, ID, USA;* [c]*Department of Mathematics and Computer Science, University of Warmia and Mazury, Olsztyn, Poland;* [d]*Department of Mathematics, Boise State University, Boise, ID, USA*

(*Received 26 October 2007; final version received 30 May 2008*)

This work demonstrates that prostate tumour progression *in vivo* can be analysed by using solutions of a mathematical model supplemented by initial conditions chosen according to growth rates of cell lines *in vitro*. The mathematical model is investigated and solved numerically. Its numerical solutions are compared with experimental data from animal models. The numerical results confirm the experimental results with the growth rates *in vivo*.

Keywords: prostate tumour progression; growth rates of Pr-cell lines *in vitro*; animal models for prostate cancer; growth rates *in vivo*; mathematical model; numerical simulations

AMS Subject Classification: 45K05; 34K28; 62P10

1. Introduction

The purpose of this paper is to analyse the C3(1)/Tag-Pr cell lines introduced in Refs. [7,12,24] and to develop a mathematical model which has a potential to describe the growth rates of Pr-cell lines *in vivo*. We have shown that the numerical solutions of the mathematical model can be used to predict the behaviour of the cancer cell (CC) populations *in vivo*.

Mathematical models of cancer growth have been the subject of research activity for many years. The models of Refs. [1–4,27] have used DNA content as a measure of the generic term 'cell size' to investigate the dynamics of the human cell cycle. For earlier studies on cell cycle dynamics, see Refs. [9,20,23,25,26]. Models which describe interactions between CCs and immune systems have been proposed, e.g. in Refs. [13–15]. Another mathematical model for tumour growth has been recently studied in Ref. [11]. This model is formulated in radial coordinates and corresponds to brain cancer progression after surgical therapy. Different initial conditions explored in Ref. [11] correspond to a small remnant of tumour tissue left after surgical resection.

In this paper, we have explored the model of Ref. [14] for the analysis of the C3(1)/Tag-Pr cell lines dynamics. The model is composed of five partial integro-differential equations. We supplement the model equations by different initial conditions which are chosen according to the experimental data described in Ref. [7]. The different Pr-cell lines *in vitro* from Ref. [7] are used as initial values for the model. Our goal is to solve the resulting initial-value problems and analyse their solutions, which show different progressions of tumours.

*Corresponding author. Email: zubik@diamond.boisestate.edu

ISSN 1748-670X print/ISSN 1748-6718 online

DOI: 10.1080/17486700802517518
http://www.informaworld.com

We construct numerical solutions for the initial-value problems and compare the computed approximations with the C3(1)/Tag cell lines *in vivo*, which are described in Ref. [7]. The approximations show a good agreement between the experimental data of Ref. [7] and the data predicted by the model. They also show that the cancer progression is larger in the cases of larger initial values (larger number of CCs injected) than in the cases of smaller initial values imposed as the initial conditions in the model. This confirms the correlation (illustrated in Ref. [7]) between the *in vitro* growth characteristics of the cell lines and the *in vivo* growth of tumours.

The organization of the paper is as follows. Section 2 describes *in vitro* cell growth in flasks and *in vivo* cell growth in C3(1)Tag Mice. Then the mathematical model of the cancer growth is described in Section 3. Numerical approximations to the solutions of the model are constructed in Section 4. Results of our numerical experiments are presented and compared with experimental data in Section 5. Concluding remarks and future goals are described in Section 6.

2. *In vitro* cell growth in flasks and *in vivo* cell growth in C3(1)Tag Mice

Over 210,000 men in the USA are diagnosed with prostate cancer every year [8]. Of these, 26,000 will succumb to the disease as a result of widespread metastasis to secondary organs, primarily the bones, lungs and liver [10]. These statistics suggest the need for improved early detection techniques and treatment options.

Prostate cancer progression is characterized by distinct morphological characteristics signifying various stages. Prostatic intraepithelial neoplasia (PIN) is believed to be the precursor lesion to prostate adenocarcinoma [5]. Inevitably, invasive adenocarcinoma will enter into systemic circulation and potentially develop secondary tumours as metastases. These highly aggressive, metastatic cells are the source of many complications associated with cancer in addition to the ultimate cause of death [6]. Good model systems are needed that allow for an increased understanding of the molecular alterations occurring during human prostate tumour progression.

The C3(1)/Tag transgenic mouse model of prostate cancer was developed by expressing the transforming sequences of the SV40 large T antigen (SV40 Tag) in tissues utilizing the regulatory sequences of the rat steroid binding protein C3(1) [18,19]. Prostates of transgenic mice develop low and high grade PIN from 2 to 7 months of age and adenocarcinoma after 6 months [22]. Based upon the predictable progression of tumour development in this model, a series of cell lines from C3(1)/Tag mice at different cancer stages were established, including the low-grade PIN cell line, Pr111 [24] and the high-grade PIN cell line, Pr117 [7]. Pr14 was established in tissue culture from a 6-month-old C3(1)/Tag mouse prostate and is an aggressive adenocarcinoma cell line [12]. Nude mouse studies involving the subcutaneous injection of Pr14 cells resulted in a rare lung metastasis. These lesions were isolated and established in culture as novel metastatic cell lines, Pr14C1 and Pr14C2 [7].

In both *in vitro* and *in vivo* analyses, the five cell lines could be distinguished by their growth characteristics. Using an *in vitro* proliferation assay, early passage (5–10) cells were cultured on collagen-coated flasks (Corning, NY) in mammary epithelial growth media (MEGM) (Bio-Whittaker, Walkersville, MD) supplemented with 2% fetal bovine serum (Invitrogen, Carlsbad, CA) and 4 nM of the synthetic androgen mibolerone (Sigma, St. Louis, MO) [7]. 10^4 cells/well were grown for 5 days in six-well plates, trypsinized, and counted daily using a Neubauer hemacytometer chamber (Hausser Scientific, Horsham, PA). The low-grade PIN cell line Pr111 had the lowest proliferation rate, Pr117, Pr14 and Pr14C2 had intermediate growth rates, and the metastatic Pr14C1 had the fastest rate of proliferation [7] (see Figure 1).

The *in vivo* growth rate of the cell lines correlated well with the *in vitro* results. 10^6 cells/0.2 ml saline were subcutaneously injected into 5–6 months old syngeneic C3(1)/Tag male mice [7].

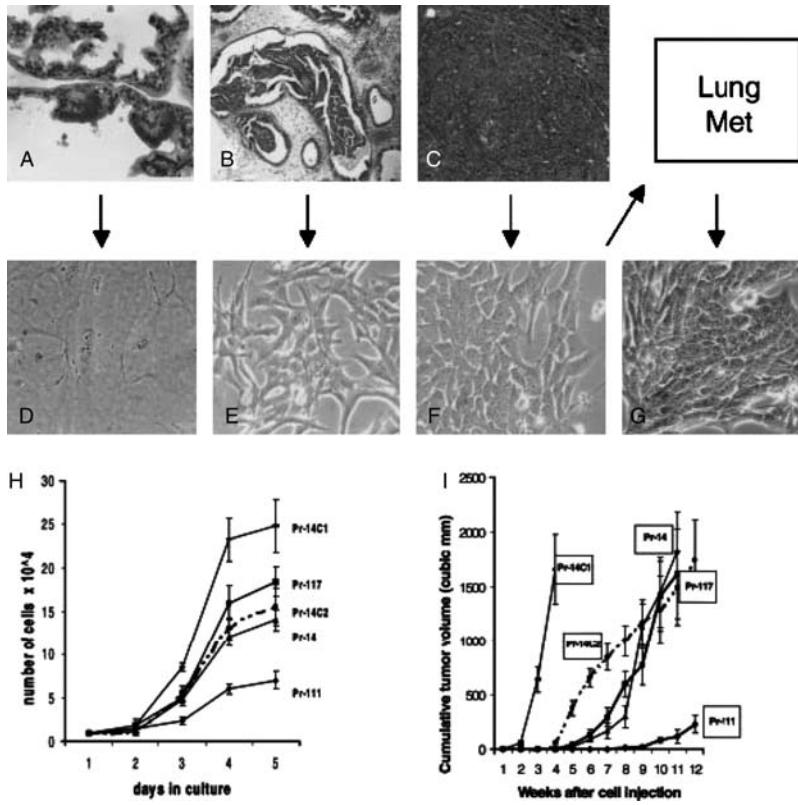

Figure 1. Morphological features and growth rates of C3(1)/Tag cell lines. *Top and middle panels*, histology of the same type of prostate lesion from which the C3(1)/Tag cell lines were isolated and morphological features of the cells in culture. A, LG-PIN-like lesions in the prostate of a 3–4-month-old C3(1)/Tag mouse. D, Pr111 cells in culture, isolated from a prostate with LG-PIN-like lesions. B, HG-PIN-like lesions in the prostate of a 5-month-old C3(1)/Tag mouse from which the Pr117 line is derived. E, Pr117 cells in culture. C, adenocarcinoma in the prostate of a C3(1)/Tag mouse. F, morphology of Pr14 cells in culture isolated from a C3(1)/Tag mouse adenocarcinoma. Cells are small and lack cytoplasm processes compared with Pr111 and Pr117. Pr14C1 and Pr14C2 cells were isolated from lung metastasis found in nude mice after injection of Pr14. G, Pr14C1 cells in culture. H, growth rates of Pr-cells line *in vitro*. Pr111 has the lowest rate of proliferation, whereas Pr14C1 has the highest rate of proliferation, with the other cells lines having intermediate rates. I, growth rates *in vivo* correlate with *in vitro* results.

Only three of five mice injected with Pr111 cells developed small tumours (<200 mm) 10–11 weeks after injection. Injection of all of the other cell lines produced large tumours that grew rapidly in five of five mice between 2 and 6 weeks after injection. Pr14C1 cells were the most aggressive [7]. These cell lines establish a model system with a cell line of low tumourigenicity (Pr111), cell lines with intermediate tumourigenicity (Pr117, Pr14 and Pr14C2), and a cell line with high tumourigenicity (Pr14C1).

3. Mathematical model

We follow the idea of Ref. [14] and investigate the development of CCs by means of mathematical equations. As in Ref. [14], we denote by

$$f_i(t,u), \quad f_i : [0,\infty)\times[0,1] \to R_+, \quad i = 1, \ldots, 6,$$

the distribution density of the ith population with activation state $u \in [0,1]$ at time $t \geq 0$. Moreover, let

$$n_i(t) = \int_0^1 f_i(t,u)\mathrm{d}u, \quad n_i : [0,\infty) \to R_+, \quad i = 1, \ldots, 6, \tag{1}$$

be the concentration of the ith cells at time $t \geq 0$. Here, the subscript $i = 1$ refers to the CCs. The other five populations described in our model are the helper T cells (Th), denoted by the subscript $i = 2$, the cytotoxic T lymphocytes (CTLs), denoted by the subscript $i = 3$, the antigen presenting cells (APCs), denoted by the subscript $i = 4$, the antigen-loaded APCs ([Ag-APC]), denoted by the subscript $i = 5$, and the cells of the host environment (HE), denoted by the subscript $i = 6$.

Here, the activation state of a given CC denotes the probability of recognition of this CC by APCs. The higher the probability, the higher is the possibility of the immune system to perform effective destruction of the tumour cell. On the contrary, if the activation state of a CC is small ($u \approx 0$) then the CC is 'invisible' for the APCs, e.g. due to antigenic modulation [16] (the disappearance of detectable tumour-specific antigens from the surface of the CC). Therefore, the smaller the activation state of a CC, the more dangerous is the tumour cell.

In our model, the activation state of a given CTL is defined as the probability of the destruction of a recognized CC after the interaction with the given CTL. The population of Th cells is involved in the activation and the proliferation of immune cells (e.g. APCs, CTLs, Th cells, B cells) by the production and the secretion of cytokines leading to the generation and the activation of immune cells [17]. In our model, the activation state of a given Th cell is defined as the quantity of cytokines produced by the Th cell after its interaction with [Ag-APC], normalized with respect to the maximal possible production of cytokines.

We take into account only binary cell interactions which are supposed to be homogeneous in space and without time delay. These encounters may change the activation state of cells as well as create or destroy cells. The activation states of the populations denoted by $i \in \{1,2,3\}$ are allowed all possible values $u \in [0,1]$. For example, we describe the possible decrease in the states of activity of CCs by the parameter $t_{16}^{(1)}$ as well as the possible increase in the activation states of Th cells and CTLs by the parameters $t_{25}^{(3)}$ and $t_{23}^{(3)}$, respectively (and the corresponding terms in Equations (2)–(4) below).

As a simplification of the biological reality, we admit the following assumptions. For the populations denoted by $i = 4$, 5 and 6, we neglect the possible change of their activity and assume that only some fixed state of activation (say $u = 0.5$) is possible. The distribution function f_6 of the HE is assumed to be constant in time. Table 1 shows the populations variables and their abbreviations for $i = 1, \ldots, 6$.

Our model describes the cellular immune response against cancer [16]. The following interactions are taken into account. We assume that the interactions between CCs and HE lead to

Table 1. Cancer-immune system dynamics variables.

Variable i	Abbreviation	Population	Activation state $u \in [0, 1]$
1	CC	Cancer cells	Recognition of CC by APC
2	Th	Helper T cells	Cytokines produced by Th cells
3	CTL	Cytotoxic T lymphocytes	Destruction of CC
4	APC	Antigen presenting cells	0.5
5	[Ag-APC]	Antigen-loaded APCs	0.5
6	HE	Host environment cells	0.5 and f_6 constant

the production of new CCs as well as to decreasing the possibility of the immune system to recognize the CCs (thus they become more dangerous). The production of new CCs is assumed to be proportional to the number of existent CCs. The respective gain term is

$$p_{16}^{(1)} \int_0^1 f_1(t, v) \mathrm{d}v.$$

Here, the subscripts 1 and 6 denote that the parameter $p_{16}^{(1)}$ corresponds to interactions between populations $i = 1$ and $i = 6$ leading to generation of cells belonging to population $i = 1$ (superscript 1). Hereafter, the respective parameters are supplied with subscripts and superscripts in a similar way.

The activation state of CCs decreases and this change of activity is described by the term

$$t_{16}^{(1)} \left(2u \int_u^1 f_1(t, v) \mathrm{d}v - u^2 f_1(t, u) \right).$$

Specific Th1 cells and CTLs are involved in the elimination of CCs. We assume that the number of destroyed CCs is proportional to the activation states of Th cells and CTLs and the respective loss terms are

$$d_{1i} f_1(t, u) \int_0^1 v f_i(t, v) \mathrm{d}v, \quad i = 2, 3, \ \ u \in [0, 1],$$

see Ref. [14] for more details. Thus we obtain the equation

$$\begin{aligned} \frac{\partial f_1}{\partial t}(t, u) =& p_{16}^{(1)} \int_0^1 f_1(t, v) \mathrm{d}v + t_{16}^{(1)} \left(2u \int_u^1 f_1(t, v) \mathrm{d}v - u^2 f_1(t, u) \right) \\ & - d_{12} f_1(t, u) \int_0^1 v f_2(t, v) \mathrm{d}v - d_{13} f_1(t, u) \int_0^1 v f_3(t, v) \mathrm{d}v, \end{aligned} \tag{2}$$

for the time evolution of the CCs.

In our model, the time evolution of the populations $i = 2$ and 3 depends on the following factors: the constant production of T cells (Th cells and CTLs) by HE, the generation of T cells as well as the increasing of the activation states of Th cells and CTLs due to the interactions between Th cells and [Ag-APC], the destruction of T cells resulting from their interactions with CCs, the natural death of T cells and the possible inlet of T cells.

There are observations that the HE constantly produces T cells and APCs [17]. The activity of newly generated T cells is small and it increases during their development and selection [16]. We model the process of the production of Th cells and CTLs by the gain terms

$$p_{16}^{(i)}(1 - u), \quad i = 2, 3.$$

The interactions between Th cells and [Ag-APC] induce a generation of new Th cells and CTLs. We assume that the rate of this production is proportional to the activation states of Th cells and that the probability of creation of very active T cells is less than the probability of the

creation of less active T cells. The respective gain terms are

$$p_{25}^{(i)}(1-u)n_5(t)\int_0^1 vf_2(t,v)\mathrm{d}v, \quad u\in[0,1], \ \ i=2,3.$$

The interactions between Th cells and [Ag-APC] lead to an increase in the activation states of Th cells and CTLs. We assume that the change of the activity of Th cells depends on the number of [Ag-APC] and is described by the term

$$t_{25}^{(2)}n_5(t)\left(2\int_0^u (u-v)f_2(t,v)\mathrm{d}v-(1-u)^2f_2(t,u)\right).$$

We assume that the change of the activity of CTLs depends on the number of Th cells and is described by the term

$$t_{23}^{(3)}\left(2\int_0^u (u-v)f_3(t,v)\mathrm{d}v-(1-u)^2f_3(t,u)\right)\int_0^1 f_2(t,v)\mathrm{d}v.$$

The interactions between T cells and CCs may result in apoptosis of Th cells and CTLs [17]. We assume that the respective loss terms for the populations $i=2$ and 3 are

$$d_{i1}f_i(t,u)\int_0^1 f_1(t,v)\mathrm{d}v, \quad i=2,3.$$

The natural death of Th cells and CTLs is described by the terms

$$d_{i6}f_i(t,u), \quad i=2,3,$$

and the possible influx of Th cells and CTLs is described by

$$S_i(t,u), \quad i=2,3.$$

In this way, we obtain

$$\begin{aligned}\frac{\partial f_2}{\partial t}(t,u)&=p_{16}^{(2)}(1-u)+p_{25}^{(2)}(1-u)n_5(t)\int_0^1 vf_2(t,v)\mathrm{d}v-d_{21}f_2(t,u)\int_0^1 f_1(t,v)\mathrm{d}v\\&\quad-d_{26}f_2(t,u)+t_{25}^{(2)}n_5(t)\left(2\int_0^u (u-v)f_2(t,v)dv-(1-u)^2f_2(t,u)\right)+S_2(t,u)\end{aligned} \tag{3}$$

and

$$\begin{aligned}\frac{\partial f_3}{\partial t}(t,u)&=p_{16}^{(3)}(1-u)+p_{25}^{(3)}(1-u)n_5(t)\int_0^1 vf_2(t,v)\mathrm{d}v-d_{31}f_3(t,u)\int_0^1 f_1(t,v)dv\\&\quad+t_{23}^{(3)}\left(2\int_0^u (u-v)f_3(t,v)\mathrm{d}v-(1-u)^2f_3(t,u)\right)\int_0^1 f_2(t,v)\mathrm{d}v-d_{36}f_3(t,u)+S_3(t,u),\end{aligned} \tag{4}$$

for the time evolution of the populations $i=2$ and 3, respectively.

For the time evolution of the fourth population of APCs, we assume their constant production by HE described by the term $p_{16}^{(4)}$ as well as production of APCs due to the interactions between Th cells and [Ag-APC] with a rate proportional to the state of activity of Th cells

described by the term

$$p_{25}^{(4)} n_5(t) \int_0^1 v f_2(t, v) \mathrm{d}v.$$

A part of APCs is loaded with cancer antigens due to the interactions between APCs and CCs [16]. We assume that the concentration of new [Ag-APC] is proportional to the state of activity of CCs and is described by the term

$$b_{14}^{(5)} n_4(t) \int_0^1 v f_1(t, v) \mathrm{d}v.$$

We note that this term is a loss term for the fourth population of APCs and it is a gain term for the fifth population of [Ag-APCs]. Taking into account also the natural death process of APCs described by the term

$$d_{46} n_4(t),$$

we obtain the equation

$$\frac{\mathrm{d}}{\mathrm{d}t} n_4(t) = p_{16}^{(4)} + p_{25}^{(4)} n_5(t) \int_0^1 v f_2(t, v) \mathrm{d}v - b_{14}^{(5)} n_4(t) \int_0^1 v f_1(t, v) \mathrm{d}v - d_{46} n_4(t) \tag{5}$$

for the time evolution of the population $i = 4$.

We also consider the possible source term $S_5(t)$ of [Ag-APC], the natural death of [Ag-APCs] described by the term

$$d_{56} n_5(t)$$

as well as their destruction by CCs described by the term

$$d_{51} n_5(t) \int_0^1 f_1(t, v) \mathrm{d}v.$$

This leads to the equation

$$\frac{\mathrm{d}}{\mathrm{d}t} n_5(t) = b_{14}^{(5)} n_4(t) \int_0^1 v f_1(t, v) \mathrm{d}v - d_{51} n_5(t) \int_0^1 f_1(t, v) \mathrm{d}v - d_{56} n_5(t) + S_5(t), \tag{6}$$

for the time evolution of the population $i = 5$.

The entire model (2)–(6) for the interacting populations is a system of partial integro-differential equations. Note that (2)–(6) is not complete and has to be supplemented by initial conditions. We apply the experimental data of Ref. [7] for the initial conditions and choose different Pr−cell lines *in vitro* as initial values. The values of the parameters of the model can be found by using experimental data and numerical approximations to the solutions of (2)–(6). The approximations are constructed in Section 4.

4. Approximate solution of the model

The purpose of this section is to construct a numerical solution to the concentrations of cells $n_j(t)$, $j = 1, \ldots, 5$, at any time variable $t > 0$. The concentrations $n_1(t)$, $n_2(t)$ and $n_3(t)$ can be computed from (1) by using the functions $f_1(t, u)$, $f_2(t, u)$ and $f_3(t, u)$. To compute numerical

approximations to the values $f_1(t,u)$, $f_2(t,u)$, $f_3(t,u)$, $n_4(t)$ and $n_5(t)$, we discretize the system (2)–(6) with respect to the activation state $u \in [0,1]$ by applying the uniform grid-points

$$u_i = i\Delta u, \quad i = 0, \ldots, N,$$

where N is a positive integer and $\Delta u = 1/N$. Then the values $f_1(t,u)$, $f_2(t,u)$ and $f_3(t,u)$ in (2)–(6) can be replaced by their approximations

$$f_j(t,u_i) \approx f_{j,i}(t), \quad j = 1,2,3, \tag{7}$$

at the state grid-points $u_i \in [0,1]$. Similarly, the values $S_2(t,u)$ and $S_3(t,u)$ can be replaced by the approximations

$$S_j(t,u_i) \approx S_{j,i}(t), \quad j = 2,3. \tag{8}$$

For every $t > 0$ and every $u_i \in [0,1]$ with $i = 0, \ldots, N$, we apply the approximations (7) for quadrature formulas to approximate the integrals:

$$\begin{gathered}\int_0^1 f_j(t,v)\mathrm{d}v \approx Q_0^N[f_j(t,v)], \quad j = 1,2, \quad \int_0^1 v f_j(t,v)\mathrm{d}v \approx Q_0^N[v f_j(t,v)], \quad j = 1,2,3,\\ \int_{u_i}^1 f_1(t,v)\mathrm{d}v \approx Q_i^N[f_1(t,v)], \quad \int_0^{u_i} (u_i - v) f_j(t,v)\mathrm{d}v \approx Q_0^i[(u_i - v) f_j(t,v)], \quad j = 2,3.\end{gathered} \tag{9}$$

The approximations in (9) represent arbitrary quadratures. For example, in Section 5, the values $Q_0^N[f_j(t,v)]$, $Q_0^N[v f_j(t,v)]$, $Q_i^N[f_1(t,v)]$ and $Q_0^i[(u_i - v) f_j(t,v)]$ are computed by the composite trapezoidal rule.

The approximations (7), (8) and (9) applied to the partial integro-differential system (2)–(6) result in the following system of ordinary differential equations:

$$\begin{cases}
\frac{\mathrm{d}f_{1,i}}{\mathrm{d}t}(t) = p_{16}^{(1)} Q_0^N\big[f_1(t,v)\big] + t_{16}^{(1)}\big(2u_i Q_i^N[f_1(t,v)] - u_i^2 f_{1,i}(t)\big) - d_{12} f_{1,i}(t) Q_0^N[v f_2(t,v)] \\
\qquad\qquad - d_{13} f_{1,i}(t) Q_0^N[v f_3(t,v)], \\
\frac{\mathrm{d}f_{2,i}}{\mathrm{d}t}(t) = p_{16}^{(2)}(1-u_i) + p_{25}^{(2)}(1-u_i) n_5(t) Q_0^N[v f_2(t,v)] - d_{21} f_{2,i}(t) Q_0^N[f_1(t,v)] - d_{26} f_{2,i}(t) \\
\qquad\qquad + t_{25}^{(2)} n_5(t)\big(2Q_0^i[(u_i - v) f_2(t,v)] - (1-u_i)^2 f_{2,i}(t)\big) + S_{2,i}(t), \\
\frac{\mathrm{d}f_{3,i}}{\mathrm{d}t}(t) = p_{16}^{(3)}(1-u_i) + p_{25}^{(3)}(1-u_i) n_5(t) Q_0^N[v f_2(t,v)] - d_{31} f_{3,i}(t) Q_0^N[f_1(t,v)] \\
\qquad\qquad + t_{23}^{(3)}\big(2Q_0^i[(u_i - v) f_3(t,v)] - (1-u_i)^2 f_{3,i}(t)\big) Q_0^N[f_2(t,v)] - d_{36} f_{3,i}(t) + S_{3,i}(t), \\
\frac{\mathrm{d}n_4}{\mathrm{d}t}(t) = p_{16}^{(4)} + p_{25}^{(4)} n_5(t) Q_0^N[v f_2(t,v)] - b_{14}^{(5)} n_4(t) Q_0^N[v f_1(t,v)] - d_{46} n_4(t), \\
\frac{\mathrm{d}n_5}{\mathrm{d}t}(t) = b_{14}^{(5)} n_4(t) Q_0^N[v f_1(t,v)] - d_{51} n_5(t) Q_0^N[f_1(t,v)] - d_{56} n_5(t) + S_5(t).
\end{cases} \tag{10}$$

The equations in (10) are solved in Section 5. The numerical solutions $f_{j,i}(t)$, with $j = 1,2,3$ and $i = 0, \ldots, N$, are then used to compute the approximations to the functions $n_1(t)$, $n_2(t)$ and $n_3(t)$.

The approximations are computed from

$$n_j(t) \approx Q_0^N[f_j(t,v)], \quad j = 1,2,3. \tag{11}$$

5. Numerical experiments

The purpose of this section is to solve system (10) and compare its solutions with the *C*3(1)/Tag cell lines and their growth characteristics *in vivo* presented in Ref. [7], Figure 1I (see Figure 1). System (10) is not complete and needs to be supplemented by initial conditions. We apply the *C*3(1)/Tag cell lines *in vitro* presented in Ref. [7], Figure 1H (see Figure 1) as the initial values for (10). Numerical tests are performed with (10) supplemented by different initial conditions, which are selected according to Figure 1H. The initial values, for which the resulting numerical solutions fit the experimental data from Figure 1I, are listed in Table 2. The values in the second row of Table 2 are obtained by scaling the values from Figure 1H with the approximate scale $1{:}1.6 \times 10^7$.

For the numerical experiments, the composite trapezoidal rule is applied to the approximations (9) and (11). The equations in (10) are solved by the code `ode15s` from the Matlab ODE suite [21]. The numerical solutions of (10) are computed with AbsTol $= 10^{-6}$ and RelTol $= 10^{-2}$. The approximations to $f_{1,i}(t)$, with $i = 0, \ldots, N$, are then applied to (11).

In order to obtain a unique solution of the model, its parameter values have to be determined. These parameters are not known in advance and their determination is based on numerical experiments. These experiments are performed with different sets of parameters and with the initial data listed in Table 2. The resulting numerical solutions are then compared with the experimental data provided in Figure 1I. The parameter values, which minimize the differences between the numerical solution and the experimental data, are listed in Table 3.

The computed approximations to $n_1(t)$ are presented in Figure 2(b). For comparison, the experimental data from Ref. [7] are given in Figure 2(a). We assume that since the populations of the CCs increase (for each of the cell lines), their concentrations and volumes increase simultaneously. The cumulative tumour volumes in Figure 2(b) have been obtained from $n_1(t)$ by using the reverse scale $1{:}1.6 \times 10^7$ and assuming that $1\,\text{mm}^3$ of tumour includes about 80,000 CCs. From the shapes of the curves, we see that both the experimental and numerical data illustrate the *C*3(1)/Tag cell lines and their growth characteristics *in vivo*.

Figure 2 indicates that the model describes accurate growth characteristics of the Pr-cell lines *in vivo*. The numerical solutions presented in Figure 2(b) illustrate the *in vivo* tumour growth rates of the cell lines Pr111, Pr117, Pr14, Pr14C2 and Pr14C1. The Pr111 cells show low tumourigenicity, while the Pr117, Pr14 and Pr14C2 cells show intermediate tumourigenicity, and the Pr14C1 show high tumourigenicity.

The numerical solution for the growth rate of the cell line Pr111 is computed from the model (10) supplemented by the smallest initial value (the smallest *in vitro* rate of proliferation) indicated in Ref. [7] (see Figure 1). Therefore, the rate of growth indicated in Figure 2(b) for Pr111 is the smallest (the solid line close to the time axis). On the other hand, the numerical

Table 2. Initial conditions for (10).

Initial values at $t = 0$ for $u \in [0,1]$	Pr111	Pr14	Pr14C2	Pr117	Pr14C1
$f_1(0,u) = f_3(0,u) = n_5(0) =$	0.4×10^{-2}	0.9×10^{-2}	1.0×10^{-2}	1.1×10^{-2}	1.7×10^{-2}
$f_2(0,u) = n_4(0) =$	0.0	0.0	0.0	0.0	0.0

Table 3. Parameter values for different Pr-cell lines *in vivo*.

Symbol	Pr111	Pr117	Pr14	Pr14C2	Pr14C1
$p_{16}^{(1)}$	0.4545	0.7143	0.6600	0.9901	1.6667
$p_{16}^{(2)}$	0.0909	0.1429	0.0667	0.1980	0.3333
$p_{16}^{(3)}$	0.0909	0.1429	0.0667	0.1980	0.3333
$p_{16}^{(4)}$	0.0909	0.1429	0.0667	0.1980	0.3333
$p_{25}^{(2)}$	0.4545	0.7143	0.3333	0.9901	1.6667
$p_{25}^{(3)}$	0.0455	0.0714	0.0333	0.0990	0.1667
$p_{25}^{(4)}$	0.9091	1.4286	0.6667	1.9802	3.3333
$t_{16}^{(1)}$	0.9091	1.4286	0.6667	1.9802	3.3333
$t_{25}^{(2)}$	0.9091	1.4286	0.6667	1.9802	3.3333
$t_{25}^{(3)}$	0.9091	1.4286	0.6667	1.9802	3.3333
$b_{14}^{(5)}$	2.0907	3.2854	1.5332	4.5540	7.6659
d_{12}	0.9091	1.4286	0.6667	1.9802	3.3333
d_{13}	0.0909	0.1429	0.0667	0.1980	0.3333
d_{21}	0.0909	0.1429	0.0667	0.1980	0.3333
d_{26}	0.0	0.0	0.0	0.0	0.0
d_{31}	0.0091	0.0143	0.0067	0.0198	0.0333
d_{36}	0.0	0.0	0.0	0.0	0.0
d_{46}	0.0	0.0	0.0	0.0	0.0
d_{51}	0.0909	0.1429	0.0667	0.1980	0.3333
d_{56}	0.0	0.0	0.0	0.0	0.0
S_2, S_3, S_5	0.0	0.0	0.0	0.0	0.0

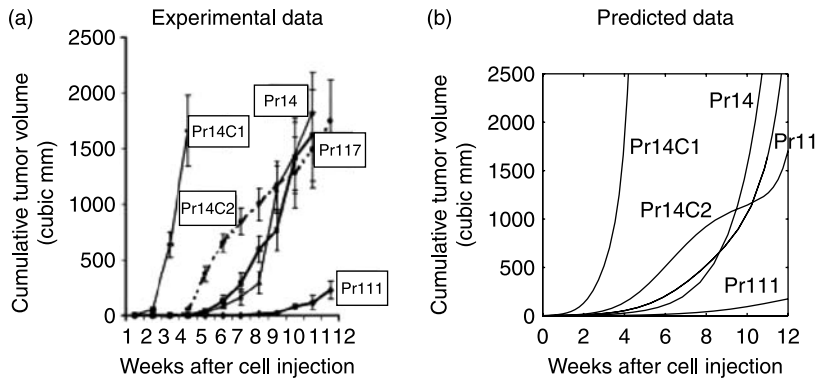

Figure 2. Experimental versus predicted data. (a) Experimental data, (b) predicted data.

solution for the growth rate of the cell line Pr14C1 is computed from (10) with the largest initial value (the largest *in vitro* rate of proliferation) indicated in Ref. [7] and the rate of growth shown in Figure 2(b) for Pr14C1 is the largest.

The numerical solutions for the growth rates of Pr117, Pr14 and Pr14C2 are presented in Figure 2(b) by the dotted, dash-dotted and dashes lines, respectively. These numerical solutions are computed from the model (10) supplemented by the initial values chosen from Ref. [7] for Pr117, Pr14 and Pr14C2, respectively. These initial values are intermediate between the initial

values for Pr111 and Pr14C1 and the corresponding numerical solutions for Pr117, Pr14 and Pr14C2 are intermediate between the numerical solutions of Pr111 and Pr14C1.

The numerical results presented in Figure 2(b) confirm the experimental results of Ref. [7] and show that the *in vitro* growth characteristics of cell lines correlate well with the *in vivo* growth of tumours.

6. Concluding remarks

We have presented a correlation between numerical and experimental results. The numerical results have been obtained by solving a system of partial integro-differential equations. Growth rates of prostate CC lines *in vitro* have been used as initial values for the initial conditions supplementing the model equations. The numerical approximations to the solutions of the resulting model have shown a good agreement with *in vivo* growth of tumours. Different kinds of tumourigenic cell lines have been illustrated by the numerical solutions of the mathematical model. The numerical results have confirmed the experimental results by showing that growth rates *in vivo* correlate with growth rates *in vitro*.

It would be interesting to develop a strategy for approximating exact amounts of CCs in different kinds of tumours. Therefore, our future work will address the exact relation between the concentrations and volumes of tumours. Another interesting open question related to the previous, which we plan to study, concerns quantitative and qualitative analysis of metastases. We will also address an efficient algorithm for finding precise parameter values for the model equations. For this algorithm, we will adopt our method presented in this paper. The method will be used to compute numerical solutions for the model with different parameter values. The numerical solutions will then be compared with the experimental data to compute their errors. In order to obtain the model outputs as close as possible to the experimental data, we will minimize the sum of the squared errors.

Acknowledgements

MK acknowledges research support from the EU project 'Modeling, Mathematical Methods and Computer Simulation of Tumour Growth and Therapy' – Contract No MRTN-CT-2004-503661. The authors wish to express their gratitude to anonymous referees for their useful comments which led to the improvements in the presentation of results and inclusion of additional Tables 1–3.

Notes

1. Email: jackiewi@math.la.asu.edu
2. Email: cjorcyk@boisestate.edu
3. Email: kolev@matman.uwm.edu.pl
4. Email: zubik@math.boisestate.edu

References

[1] B. Basse, B.C. Baguley, E.S. Marshall, W.R. Joseph, B. van Brunt, G.C. Wake, and D.J.N. Wall, *A mathematical model for analysis of the cell cycle in cell lines derived from human tumours*, J. Math. Biol. 47 (2003), pp. 295–312.

[2] ———, *Modelling cell death in human tumour cell lines exposed to the anticancer drug paclitaxel*, J. Math. Biol. 49 (2004), pp. 329–357.

[3] B. Basse, B.C. Baguley, E.S. Marshall, G.C. Wake, and D.J.N. Wall, *Modelling cell population growth with applications to cancer therapy in human tumour cell lines*, Prog. Biophys. Mol. Biol. 85 (2004), pp. 353–368.

[4] ———, *Modelling the flow cytometric data obtained from unperturbed human tomour cell lines: Parameter fitting and comparison*, Bull. Math. Biol. 67(4) (2005), pp. 815–830.
[5] D.G. Bostwick, A. Pacelli, and A. Lopez-Beltran, *Ultrastructure of prostatic intraepithelial neoplasia*, Prostate 33 (1997), pp. 32–37.
[6] D.G. Bostwick and J. Qian, *Effect of androgen deprivation therapy on prostatic intraepithelial neoplasia*, Urology 58 (2001), pp. 91–93.
[7] A. Calvo, N. Xiao, J. Kang, C.J.M. Best, I. Leiva, M.R. Emmert-Buck, C. Jorcyk, and J.E. Green, *Alterations in gene expression profiles during prostate cancer progression: Functional correletions to tumorigenicity and down-regulation of selenoprotein-P in mouse and human tumors*, Cancer Res. 62 (2002), pp. 5325–5335.
[8] Cancer Statistics, American Cancer Society, Inc., Atlanta, 57(1) (2007), pp. 43–66.
[9] I. Hoffman and E. Karsenti, *The role of cdc25 in checkpoints and feedback controls in the eukaryotic cell cycle*, J. Cell Sci. Suppl. 18 (1994), pp. 75–79.
[10] J.L. Holleran, C.J. Miller, N.L. Edgehouse, T.P. Pretlow, and L.A. Culp, *Differential experimental micrometastasis to lung, liver, and bone with lacZ-tagged CWR22R prostate carcinoma cells*, Clin. Exp. Metastasis 19 (2002), pp. 17–24.
[11] Z. Jackiewicz, Y. Kuang, C. Thalhauser, and B. Zubik-Kowal, *Numerical solution of a model for brain cancer progression after therapy*, submitted.
[12] C.L. Jorcyk, M.-L. Liu, M.-A. Shibata, I.G. Maroulakou, K.L. Komschlies, M.J. McPhaul, J.H. Resau, and J.E. Green, *Development and characterization of a mouse prostate adenocarcinoma cell line: Ductal formation determined by extracellular matrix*, Prostate 34 (1998), pp. 10–22.
[13] M. Kolev, *Mathematical modeling for the competition between acquired immunity and cancer*, Int. J. Appl. Math. Comput. Sci. 13(3) (2003), pp. 289–296.
[14] ———, *A mathematical model of cellular immune response to leukemia*, Math. Comput. Model. 41 (2005), pp. 1071–1081.
[15] M. Kolev, E. Kozłowska, and M. Lachowicz, *A mathematical model for single cell cancer-immune system dynamics*, Math. Comput. Model. 41 (2005), pp. 1083–1095.
[16] J. Kuby, *Immunology*, 3rd ed., W.H. Freeman, New York, 1997.
[17] P.M. Lydyard, A. Whelan, and M.W. Fanger, *Instant Notes in Immunology*, BIOS Scientific Publishers Ltd, Oxford, 2000.
[18] I.G. Maroulakou, M. Anver, L. Garrett, and J.E. Green, *Prostate and mammary adenocarcinoma in transgenic mice carrying a rat C3(1) simian virus 40 large tumor antigen fusion protein*, Proc. Natl. Acad. Sci. USA 91 (1994), pp. 11236–11240.
[19] M.G.R. Parker, H. White, M. Hurst, M. Needham, and R. Tilly, *Prostatic steroid-binding protein: Isolation and characterization of C3 genes*, J. Biol. Chem. 258 (1983), pp. 12–15.
[20] D.M. Prescot, *Cell reproduction*, Int. Rev. Cytol. 100 (1987), pp. 93–128.
[21] M.W. Shampine and M.W. Reichelt, *The Matlab ODE suite*, SIAM J. Sci. Comput. 18 (1997), pp. 1–22.
[22] M.-A. Shibata, C.L. Jorcyk, M.-L. Liu, K. Yoshidome, L.G. Gold, and J.E. Green, *The C3(1)/SV40 T antigen transgenic mouse model of prostate and mammary cancer*, Toxicol. Pathol. 26 (1998), pp. 177–182.
[23] J.A. Smith and L. Martin, *Do cells cycle?* Proc. Natl. Acad. Sci. USA 70 (1973), pp. 1263–1267.
[24] C.R. Soares, M.-A. Shibata, J.E. Green, and C.L. Jorcyk, *Development of PIN and prostate adenocarcinoma cell lines: A model system for multistage tumor progression*, Neoplasia 4 (2002), pp. 112–120.
[25] J.V. Watson, *Tumour growth dynamics*, Br. Med. Bull. 47 (1991), pp. 47–63.
[26] G.D. Wilson, N.J. McNally, S. Dische, M.I. Saunders, C. Des Rochers, A.A. Lewis, and M.H. Bennet, *Measurement of cell kinetics in human tumours in vivo using bromodeoxyuridine incorporation and low cytometry*, Br. J. Cancer 58 (1988), pp. 423–431.
[27] B. Zubik-Kowal, *Solutions for the cell cycle in cell lines derived from human tumors*, Comput. Math. Methods Med. 7(4) (2006), pp. 215–228.